Bloch dynamics of light waves in helical optical waveguide arrays

Stefano Longhi
Dipartimento di Fisica and Istituto di Fotonica e Nanotecnologie del CNR, Politecnico di Milano, Piazza L. da Vinci 32, I-20133 Milan, Italy

(Received 22 August 2007; published 20 November 2007)

Propagation of light waves in one-dimensional and two-dimensional photonic lattices made of uniformly twisted (helical) arrays of evanescently coupled optical waveguides is theoretically investigated and shown to provide a classic wave optics analog of the quantum dynamics of a Bloch particle in an electromagnetic field. For a one-dimensional waveguide array, it is demonstrated that the behavior of discretized light in the array exactly mimics the wave packet dynamics of a quantum harmonic oscillator on a lattice, with the existence of quasiharmonic and quasi-Bloch oscillations. For a two-dimensional twisted waveguide array, it is shown that propagation of discretized light exactly mimics the quantum motion of an electron in a two-dimensional crystalline potential subjected to a uniform magnetic field, orthogonal to the crystal plane, combined with a repulsive harmonic electrostatic force.

DOI: 10.1103/PhysRevB.76.195119 PACS number(s): 72.10.Bg, 72.90.+y, 42.82.Et

I. INTRODUCTION

The study of discretized light in photonic lattices, such as in arrays of evanescently coupled optical waveguides,[1,2] has in recent years received continuous and increasing interest from both fundamental and applied viewpoints.[3,4] It has been pointed out on several occasions that the tunneling dynamics of classic light waves in coupled waveguides closely resembles the quantum dynamics of an electron in crystalline potentials (see, for instance, Refs. 3 and 4). In particular, using properly engineered photonic lattices, one can simulate with light waves the coherent motion of a Bloch electron subjected to an external dc or ac electric field (see, for instance, Refs. 5–10). As the monitoring of the electron motion in crystals is a complicated task and unavoidable dephasing and many-body effects may even prevent the observation of coherent dynamical effects, visualization of optical beam reshaping can be performed with great accuracy (see, for instance, Refs. 11–13), making photonic lattices a rather unique laboratory tool to investigate in real space coherent wave packet dynamics. Such a remarkable possibility has been successfully exploited to experimentally investigate in photonic lattices the classic wave optics analogs of a variety of coherent phenomena originally predicted for electrons in crystalline potentials subjected to a static or time-periodic electric field, including Bloch oscillations,[7,8,11,12,14,15] Zener tunneling,[11,14–16] and dynamic localization.[17–19] A powerful means to simulate in one- or two-dimensional periodic optical structures the effect of a constant or time-dependent electric field in the corresponding quantum mechanical problem is to bend the array in the longitudinal direction.[6,9,10,17,20–22] In fact, in the reference frame of the waveguides the bending of the array introduces a noninertial force which is related to the local waveguide curvature by a Newtonian equation of motion.[10,23] Diffraction control and the optical analogs of Bloch dynamics based on bent waveguides have been experimentally demonstrated for one-dimensional waveguide arrays in Refs. 12 and 17–20. Recent advances in the manufacturing of two-dimensional high-precision fiber waveguide arrays[24] and of periodic waveguide structures of arbitrary two-dimensional geometry by using femtosecond laser writing[25–27] have also motivated theoretical investigations on discretized light behavior in two-dimensional photonic lattices with an arbitrary complex bending shape.[22] On the other hand, an outstanding problem of solid state physics is to understand the motion of electrons in a crystalline potential under the action of a *magnetic field*, or more generally of combined electric and magnetic fields (see, for instance, Refs. 28 and 29), a problem which dates back to the fundamental works by Bloch,[30] Jones and Zener,[31] Peierls[32] and later on put on a more rigorous basis by Slater[33] for electric fields and by Luttinger[34] for magnetic fields using a Wannier function expansion technique (for a review, see for instance, Ref. 35). In particular, the problem of two-dimensional Bloch electrons in an applied magnetic field has been intensively studied for several decades and related to various phenomena such as the quantum Hall effect or superconductivity in the presence of magnetic field. In the simplest semiclassical approximation, which is valid for suitable wave packets which are spread over many lattice spacings and for weak external fields, the electron dynamics subjected to slowly varying external scalar and vector potentials is that of a classical charged particle with an effective Hamiltonian in which the crystalline potential is simply accounted for by replacing the free kinetic energy term by an energy band of the crystal. The ability offered by optics to visualize in the real space the wave packet dynamics of a corresponding quantum Bloch particle motivates to extend previous optical analogs of one-dimensional or two-dimensional Bloch motion in dc or ac electric fields[6,9,10,12,17,19] to include the effect of a magnetic field.

In this work, we study theoretically the propagation of light waves in one-dimensional and two-dimensional periodic arrays of weakly coupled waveguides which are uniformly *twisted* in the longitudinal direction, and show that the reshaping of an optical beam is analogous to the coherent dynamics of an electronic wave packet in a crystalline potential subjected to a uniform magnetic field, orthogonal to the crystal plane, superimposed to an electrostatic inverted parabolic potential. The geometric twist of the optical structure along the propagation direction is in fact responsible for

the appearance, in the reference frame of the waveguides, of noninertial Coriolis and centrifugal forces (see, for instance, Refs. 36 and 37), which are analogous the former to a magnetic (Lorentz) force and the latter to an electrostatic (repulsive) harmonic force. In the one-dimensional array, the magnetic field does not influence the wave packet dynamics and the twisted one-dimensional optical lattice mimics the dynamics of a quantum harmonic oscillator on a lattice,[38–40] which has received a great interest in the past recent years after its realization in Bose-Einstein condensates.[41–45] In our case, in spite of the fact that the harmonic oscillator is actually *inverted*, owing to the discrete translational invariance of the lattice and thus of the periodicity of the band structure, we retrieve the same dynamical scenario as in a confining harmonic potential on a lattice. In the semiclassical limit, the beam dynamics is governed by a pendulum equation, with the existence of two different kinds of orbits corresponding to harmonic and Bloch oscillations. Owing to nonequidistant spectrum, these oscillations are, however, damped (the optical analog of quantum mechanical dephasing). In the twisted two-dimensional array, the wave packet dynamics is more involved since the magnetic (Coriolis) force acts in addition to the two-dimensional electrostatic (centrifugal) force. The beam trajectory, as predicted by a semiclassical analysis, follows a complex flowerlike path in the transverse plane, which is again smeared out owing to quantum mechanical dephasing.

The paper is organized as follows. In Sec. II, the basic equations describing light propagation in a helical array of weakly coupled optical waveguides is presented, and the optical-quantum analogy between spatial beam propagation along the array and coherent temporal evolution of a Bloch electron in an electromagnetic field is highlighted. Section III deals with the case of a one-dimensional helical array, where discretized light behaves similarly to a quantum harmonic oscillator on a lattice. Beam dynamics in a two-dimensional helical waveguide array is considered in Sec. IV, and the results predicted by the semiclassical analysis are compared with full numerical simulations of the paraxial wave equation. Finally, in Sec. V, the main conclusions are outlined.

II. LIGHT PROPAGATION IN HELICAL WAVEGUIDE ARRAYS: GENERAL ASPECTS

A. Basic model and quantum-optical correspondence

The starting point of our analysis is provided by a rather standard model describing propagation of monochromatic light waves at wavelength λ in an array of weakly coupled optical waveguides which is uniformly twisted along the propagation direction Z with a spatial twist period Λ. In the weak guidance approximation, where the refractive index $n(X,Y,Z)$ of the optical structure weakly deviates from the substrate (cladding) index n_s,[46] the scalar and paraxial field approximations can be used and propagation of the electric field envelope $\psi(X,Y,Z)$, in a given polarization state, is governed by the Schrödinger-like wave equation (see, for instance, Refs. 17, 19, 22, and 36),

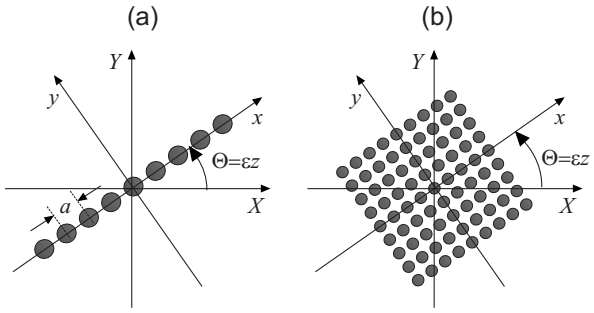

FIG. 1. Schematic of (a) one-dimensional and (b) two-dimensional (square lattice) uniformly twisted waveguide arrays. The reference frame (x,y) of the waveguide structure uniformly rotates along the propagation z direction with a rate $d\Theta/dz=\epsilon=2\pi/\Lambda$, where Λ is the helical pitch.

$$i\lambda\frac{\partial\psi}{\partial Z}=-\frac{\lambda^2}{2n_s}\nabla_{X,Y}^2\psi+V(X,Y,Z)\psi, \tag{1}$$

where X, Y, and Z are the Cartesian spatial coordinates in the laboratory reference frame, $\nabla_{X,Y}^2=(\partial^2/\partial X^2)+(\partial^2/\partial Y^2)$ is the transverse Laplacian, $\lambda=\lambda/(2\pi)$ is the reduced wavelength, and $V(X,Y,Z)=[n_s^2-n^2(X,Y,Z)]/(2n_s)\simeq n_s-n(X,Y,Z)$ is the optical potential. The formal optical-quantum correspondence between light propagation along the optical structure and the temporal evolution of a nonrelativistic quantum particle constrained to move on the two-dimensional (X,Y) plane is readily obtained by replacing the temporal variable t in the quantum problem with the spatial propagation distance Z in the optical system, the Planck constant $\hbar$ with the reduced wavelength λ, the particle mass m with the substrate refractive index n_s, and the time-dependent quantum potential $V(X,Y,t)$ with the Z-dependent optical potential $V(X,Y,Z)$. To study light propagation along the helical arrayed structure, it is worth introducing a rotating reference frame (x,y,z) that follows the twist of the structure (see, for instance, Ref. 36),

$$x=X\cos\Theta+Y\sin\Theta,\quad y=-X\sin\Theta+Y\cos\Theta,\quad z=Z, \tag{2}$$

where $\Theta(z)=\int_0^z\epsilon(\xi)d\xi=\epsilon z$ and $\epsilon=2\pi/\Lambda$ is the (uniform) twist rate (see Fig. 1). In the rotating reference frame (x,y,z), the optical structure turns out to be invariant along z and the wave equation [Eq. (1)] takes the form

$$i\lambda\frac{\partial\psi}{\partial z}=-\frac{\lambda^2}{2n_s}\nabla_{x,y}^2\psi+V(x,y)\psi-\epsilon\mathcal{L}_z\psi, \tag{3}$$

where

$$\mathcal{L}_z\equiv i\lambda\left(y\frac{\partial}{\partial x}-x\frac{\partial}{\partial y}\right) \tag{4}$$

is the component of the angular momentum operator along the z direction. The equivalence between Eq. (3) and the two-dimensional nonrelativistic Schrödinger equation for a particle of mass n_s and charge q in the periodic potential $V(x,y)$, subjected to time-independent electric and magnetic

fields derived from the vector and scalar potentials $\mathbf{A}$ and φ, is readily established by observing that Eq. (3) can be cast in the equivalent form

$$i\lambda\frac{\partial\psi}{\partial z}=\frac{1}{2n_s}\sum_{k=x,y}(p_k-qA_k)^2\psi+V(x,y)\psi+q\varphi\psi, \qquad (5)$$

where $p_x=-i\lambda\partial/\partial x$, $p_y=-i\lambda\partial/\partial y$ are the momentum operators, and where we have set

$$q\mathbf{A}(x,y)=n_s\epsilon(-y\mathbf{u}_x+x\mathbf{u}_y), \quad q\varphi(x,y)=-\frac{n_s\epsilon^2}{2}(x^2+y^2) \qquad (6)$$

for the vector and scalar potentials. Note that the corresponding magnetic field $\mathbf{B}=\nabla\times\mathbf{A}$ is uniform and orthogonal to the (x,y) plane of motion, whereas the electric field $\mathbf{E}=-\nabla\varphi$ corresponds to an elastic repulsive force. Note also that the classic magnetic and electric forces experienced by the particle of mass n_s in the electromagnetic field, given by $\mathbf{F}_m=q\mathbf{v}\times\mathbf{B}$ and $\mathbf{F}_e=q\mathbf{E}$, are nothing else than the Coriolis and centrifugal forces appearing in the noninertial rotating reference frame (x,y,z). Therefore, the twist of the optical structure along the propagation z direction introduces, in addition to an electric force as in case of bending previously studied in Refs. 6, 9, 10, 17, and 22, a magnetic force which depends on the particle velocity. The effect of the twist on discretized light propagation along the array turns out to strongly depend on the dimensionality of the array. In the case of a one-dimensional array of weakly coupled waveguides placed, e.g., along the x axis, the magnetic force is orthogonal to the array line and it is not expected therefore to influence discrete light diffraction, which is ruled by the interplay between the periodic optical potential in the x direction and the repulsive (inverted) one-dimensional harmonic potential due to the centrifugal force. As shown in Sec. III, this optical system provides a remarkable example in classic wave optics to investigate the coherent dynamics of a quantum harmonic oscillator on a lattice.[38,39] Conversely, for a two-dimensional array of waveguides, the reshaping of a light beam results from the interplay between the periodic lattice, the magnetic force, and the two-dimensional repulsive harmonic potential, as discussed in Sec. IV. Before discussing in details the dynamics of discretized light in one-dimensional and two-dimensional helical waveguide arrays, it should be pointed out that in the present work, we will limit ourselves to consider a sufficiently small twist rate so that a light beam in each waveguide of the array adiabatically follows its helical path. Different dynamical regimes attained at moderate or high values of the twist rates, corresponding to strong radiation losses due to the centrifugal force or to adiabatic stabilization and averaged-potential regimes (see, for instance, Refs. 47 and 48), will not be considered in the present analysis.

B. Coupled-mode equations

The formulation [Eq. (5)] of the wave propagation problem allows one to directly apply the general theory by Luttinger[34]—originally developed for electrons in periodic crystalline potentials subjected to an electromagnetic field—to study the optical beam evolution in the case of a two-dimensional periodic array of helical waveguides. This procedure will be briefly reviewed in Sec. IV. However, for nonperiodic or for a one-dimensional chain of weakly coupled waveguides, one can proceed by a suitable extension of the coupled-mode equation approach,[1,2] which is a much more common and known procedure in the optical context to study light propagation in weakly coupled waveguides. To this aim, let us consider a chain of weakly coupled and identical waveguides placed at the positions $\mathbf{R}_1=(x_1,y_1)$, $\mathbf{R}_2=(x_2,y_2),\ldots,\mathbf{R}_\rho=(x_\rho,y_\rho),\ldots$, in the (x,y) plane, and assume for the potential $V(\mathbf{r})$ the expression $V(\mathbf{r})=\Sigma_{\mathbf{R}_\rho}Q(\mathbf{r}-\mathbf{R}_\rho)$, where $\mathbf{r}=(x,y)$, $Q(\mathbf{r})\simeq n_s-n_g(\mathbf{r})$, and $n_g(\mathbf{r})$ is the refractive index profile of the single waveguide. Let $u(\mathbf{r}-\mathbf{R}_\rho)$ be the fundamental mode profile of the single waveguide centered at $\mathbf{R}_\rho$, and let us look for a solution to Eq. (5) in the form

$$\psi(\mathbf{r},z)=\sum_{\mathbf{R}_\rho}c(\mathbf{R}_\rho,z)u(\mathbf{r}-\mathbf{R}_\rho)\times\exp[i(n_s\epsilon/\lambda)(-xy_\rho+yx_\rho)]\exp(-i\beta_0 z), \qquad (7)$$

where β_0 is the propagation constant of the fundamental mode of the single waveguide and where the slow evolution of the amplitudes $c(\mathbf{R}_\rho,z)$ with z comes from the weak coupling of adjacent waveguides and from the presence of the electrostatic potential φ. Note that, as compared to the usual mode expansion approach adopted to derive coupled-mode equations in weakly coupled waveguides (see, for instance, Ref. 2), we have included in Eq. (7) the additional phase terms $\exp[i(n_s\epsilon/\lambda)(-xy_\rho+yx_\rho)]$ which arise due to the presence of the vector potential $\mathbf{A}$ in Eq. (5). To understand such additional phase terms, let us apply the operator $\mathcal{H}_\rho=(1/2n_s)\Sigma_{k=x,y}(p_k-qA_k)^2+Q(\mathbf{r}-\mathbf{R}_\rho)$ to $w_\rho(\mathbf{r})=u(\mathbf{r}-\mathbf{R}_\rho)\exp[i(n_s\epsilon/\lambda)(-xy_\rho+yx_\rho)]$. Taking into account that $u(\mathbf{r}-\mathbf{R}_\rho)$ is strongly localized at around $\mathbf{r}\sim\mathbf{R}_\rho$, we may approximately set $q\mathbf{A}(\mathbf{r})\simeq q\mathbf{A}(\mathbf{R}_\rho)=n_s\epsilon(-y_\rho\mathbf{u}_x+x_\rho\mathbf{u}_y)$ for the vector potential entering in $\mathcal{H}_\rho$, so that one has $\mathcal{H}_\rho w_\rho(\mathbf{r})\simeq\lambda\beta_0 w(\mathbf{r})$, i.e., $w_\rho(\mathbf{r})$ is the natural eigenmode of $\mathcal{H}_\rho$. To derive the evolution equations for the mode amplitudes $c(\mathbf{R}_\rho,z)$, we follow a rather standard procedure[2] and substitute ansatz (7) into the wave equation [Eq. (5)]. This yields

$$i\lambda\sum_{\mathbf{R}_\rho}\frac{dc(\mathbf{R}_\rho,z)}{dz}w_\rho(\mathbf{r})=\sum_{\mathbf{R}_\rho}c(\mathbf{R}_\rho,z)[V(\mathbf{r})-Q(\mathbf{r}-\mathbf{R}_\rho)+q\varphi(\mathbf{r})]w_\rho(\mathbf{r}). \qquad (8)$$

Multiplying both sides of Eq. (8) by $w^*_{\rho'}(\mathbf{r})$, integrating in $d\mathbf{r}$, and taking into account the strong localization of the modes $w_\rho(\mathbf{r})$ and that $\int d\mathbf{r}w^*_{\rho'}(\mathbf{r})w_\rho(\mathbf{r})\simeq\delta_{\mathbf{R}_\rho,\mathbf{R}_{\rho'}}$, one finally obtains the following coupled-mode equations:

$$i\frac{dc(\mathbf{R}_{\rho'},z)}{dz} = -\sum_{\mathbf{R}_\rho} \Delta_{\rho'\rho} \exp(i\phi_{\rho'\rho}) c(\mathbf{R}_\rho,z) - \frac{n_s \epsilon^2 |\mathbf{R}_{\rho'}|^2}{2\chi} c(\mathbf{R}_{\rho'},z), \quad (9)$$

where we have set

$$\Delta_{\rho'\rho} = -\frac{1}{\chi}\int d\mathbf{r} u^*(\mathbf{r}-\mathbf{R}_{\rho'})[V(\mathbf{r})-Q(\mathbf{r}-\mathbf{R}_\rho)]u(\mathbf{r}-\mathbf{R}_\rho) \quad (10)$$

and

$$\phi_{\rho'\rho} = \frac{\epsilon n_s}{\chi}(-x_{\rho'}y_\rho + x_\rho y_{\rho'}) = \frac{q}{\chi}\int_{\mathbf{R}_\rho}^{\mathbf{R}_{\rho'}} \mathbf{A}(\mathbf{r})\cdot d\mathbf{r}. \quad (11)$$

The integral on the right hand side in Eq. (11) has to be performed along the straight line connecting the points $\mathbf{R}_\rho$ and $\mathbf{R}_{\rho'}$. Note that, as compared to the straight array, the change of coupled-mode equations induced by a uniform twist of the array along the propagation direction is twofold: (i) to introduce the additional phase terms $\exp(i\phi_{\rho'\rho})$ in the coupling coefficients $\Delta_{\rho'\rho}$, which are given by the Peierls integrals [Eq. (11)] for the vector potential, and (ii) to introduce a shift in propagation constants represented by the last terms on the right hand side in Eq. (9) and originating from the electrostatic (centrifugal) potential $q\varphi$.

III. LIGHT PROPAGATION IN A ONE-DIMENSIONAL HELICAL ARRAY: THE CLASSICAL ANALOG OF A QUANTUM HARMONIC OSCILLATOR ON A LATTICE

Let us consider, as a first example, the case of a one-dimensional helical waveguide array made of a chain of equal waveguides placed along the x axis at equal distances a each other [see Fig. 1(a)], so that $V(x,y)=\Sigma_n[n_s-n_g(x-na,y)]$, where n is an integer number. In this case, considering only the nearest neighboring interaction terms in the sum on the right hand side of Eq. (9) and dropping the unimportant equal shift terms $\Delta_{\rho\rho}$, the coupled mode equations [Eq. (9)] assume the simplified form

$$i\frac{dc_n}{dz} = -\Delta(c_{n+1}+c_{n-1}) - \gamma n^2 c_n, \quad (12)$$

where we have set $c_n(z)=c(\mathbf{R}_n,z)$, $\mathbf{R}_n=na\mathbf{u}_x$,

$$\Delta = \frac{1}{\chi}\int dxdy u^*(x-a,y)[n(x,y)-n_g(x,y)]u(x,y), \quad (13)$$

and

$$\gamma = \frac{\epsilon^2 n_s a^2}{2\chi}. \quad (14)$$

Note that in this case the Peierls phase terms $\exp(i\phi_{n'n})$, which account for the presence of the magnetic field, vanish. This is physically due to the fact that the magnetic (Lorentz) force is orthogonal to the (x,z) plane containing the one-dimensional waveguide array and therefore it does not influence the light transfer between adjacent waveguides of the array. In their present form, Eq. (12) is formally analogous to the discrete equations describing the dynamics of a quantum harmonic oscillator on a lattice (see Refs. 38 and 39), apart from the fact that in our case the harmonic potential is *inverted*, i.e., the harmonic force is repulsive rather than attractive. However, owing to the periodicity of the tight-binding lattice band curve, the dynamical scenario is the same in the two cases. This can be formally shown by making the substitution $c_n(z)=a_n(-z)\exp(i\pi n)$: the evolution equations for the amplitudes $a_n(z)$ are given again by Eq. (12) but with γ replaced by $-\gamma$. In the quantum physics context, a realization of a quantum harmonic oscillator on a lattice has been recently attained in Bose-Einstein condensates in a periodic optical lattice trapped by an harmonic confining potential.[41,42] The spectral and dynamical properties of a quantum harmonic oscillator on a lattice have been studied in great details, and we refer the reader to, e.g., Refs. 38–45. In particular, the eigenmodes $\bar{c}_n^\alpha$ and eigenvalues E_α of Eq. (12) $[c_n(z)=\bar{c}_n^\alpha \exp(iE_\alpha z)]$ can be expressed in terms of Mathieu functions.[38,43] A physically interesting case is that corresponding to a weak twist rate such that $\gamma \ll \Delta$, i.e., to

$$\epsilon \ll \sqrt{\frac{2\Delta\chi}{n_s a^2}}. \quad (15)$$

In this case, Eq. (12) possesses two different classes of eigenstates depending on their energy E_α and based on the localization of these modes (see, for instance, Ref. 43). The low-energy modes are extended around the $n=0$ waveguide and nearly equally separated in energy by $\Delta E_\alpha \sim 2\sqrt{\gamma\Delta}$. These are basically the discrete counterpart of the eigenstates of the continuous quantum harmonic oscillator. Conversely, the high-energy modes are localized on the two sides of the $n=0$ waveguide and correspond to pairs of nearly degenerate Wannier-Stark ladders with increasing energy spacing as the energy E_α increases.[39,42,43] The existence of such a two kinds of eigenstates is reflected into the two rather different dynamical regimes of a wave packet of the quantum harmonic oscillator on a lattice in dependence of its initial energy. This can be conveniently understood by means of a semiclassical analysis of the wave packet dynamics.[39,41,44] To this aim, let us notice that the solution to the coupled-mode equations [Eq. (12)] can be written as $c_n(z)=f(\xi=n,z)$, where the continuous function $f(\xi,z)$ satisfies the Schrödinger-like equation $i(\partial f/\partial z)=\mathcal{H}f$ with the Hamiltonian

$$\mathcal{H} = -2\Delta\cos(p_\xi) - \gamma\xi^2, \quad (16)$$

where $p_\xi=-i\partial/\partial\xi$ is the momentum operator. For the Ehrenfest theorem, the semiclassical equations for the mean values $\langle\xi\rangle$ of wave packet position (in units of the array period a) and $\langle p_\xi\rangle$ of momentum are given by

$$\frac{d\langle\xi\rangle}{dz} = \left\langle\frac{\partial\mathcal{H}}{\partial p_\xi}\right\rangle = 2\Delta\langle\sin p_\xi\rangle \simeq 2\Delta\sin\langle p_\xi\rangle, \quad (17)$$

$$\frac{d\langle p_\xi\rangle}{dz} = -\left\langle \frac{\partial \mathcal{H}}{\partial \xi} \right\rangle = 2\gamma\langle \xi\rangle. \tag{18}$$

To understand the physical meaning of the mean value of momentum $\langle p_\xi\rangle$ in our optical system, let us assume that at the input plane $z=0$, the waveguide array is excited by a broad beam in the x direction (of, e.g., Gaussian shape) tilted by a small angle θ_0 with respect to the paraxial z axis, i.e., $f(x,0)\sim|f(x,0)|\exp(\pm i\theta_0 x/\lambda)$, where the amplitude $|f(x,0)|$ is a slowly varying function of x on the spatial length of the array period a. Owing to the discreteness condition $x=na$ imposed by the lattice, θ_0 should be reported inside the interval $-\theta_B<\theta_0\leq\theta_B$, where

$$\theta_B = \frac{\lambda}{2a} \tag{19}$$

is the Bragg angle. Since $x=\xi a$, one then has $\langle p_\xi\rangle \simeq \pm\theta_0 a/\lambda$: The mean value of momentum $\langle p_\xi\rangle$ is thus proportional to the tilting angle of the optical beam with respect to the paraxial z direction. Note that at the incidence angle θ_0 equal to the Bragg angle, one has $\langle p_\xi\rangle=\pi$, and thus in general one can write $\langle p_\xi\rangle=\pm\pi(\theta_0/\theta_B)$. In terms of classic ray optics, the Hamiltonian equations [Eqs. (17) and (18)] can be viewed as the paraxial ray equations describing the propagation of optical rays in a fictitious dielectric medium, $\langle\xi\rangle$ and $(\lambda/a)\langle p_\xi\rangle$ being the spatial and angular ray displacements (see, for instance, Ref. 49). On the other hand, the semiclassical dynamics expressed by the Hamiltonian systems [Eqs. (17) and (18)] is equivalent to that of a classical pendulum. In fact, after introduction of the translated momentum $q=\langle p_\xi\rangle-\pi$ from Eqs. (17) and (18), it follows that q satisfies the pendulum equation,

$$\frac{d^2q}{dz^2} + \Omega^2 \sin q = 0, \tag{20}$$

where $\Omega=2\sqrt{\Delta\gamma}$. It is well known that the orbits of the classical pendulum depend on the value of the mechanical energy $E=(1/2)(dq/dz)^2-\Omega^2\cos q=2\gamma^2\langle\xi\rangle^2+\Omega^2\cos\langle p_\xi\rangle$, which is a constant of motion (note that $E=-2\gamma\mathcal{H}$). In particular, for $E<E_c$, the motion of the pendulum is vibrational, whereas for $E>E_c$, it is rotational, where $E_c=\Omega^2=4\gamma\Delta$. In fact, the trajectories of the dynamics in the phase space $(\langle\xi\rangle,\langle p_\xi\rangle)$, shown in Fig. 2 and calculated by numerical integration of Eqs. (17) and (18), indicate that the isoenergy ray orbits belong to two different classes, corresponding to the rotational (open orbits, for $E>E_c$) and vibrational (closed orbits, for $E<E_c$) regimes of the pendulum. The energy E of the orbit is determined by the beam launching conditions at the input plane $z=0$ of the array: if the light beam is centered at the waveguide n_0 with a tilting angle θ_0 with respect to the z axis, one has

$$E = 2\gamma^2 n_0^2 + \Omega^2\cos(\pi\theta_0/\theta_B). \tag{21}$$

Open and closed orbits are separated by a separatrix, corresponding to the orbit with energy $E=E_c$. Optical rays corresponding to closed orbits oscillate around the central waveguide $n=0$, whereas optical rays corresponding to open orbits oscillate on the sides of the central waveguide $n=0$.[50] The closed orbits are analogous of the periodic trajectories of optical rays in a parabolic graded-index lens, and in the regime of small-angle oscillations of the pendulum, the spatial period of the ray oscillations is given by $\simeq 2\pi/\Omega$. Conversely, the open orbits in the semiclassical dynamics are analogous of Bloch oscillations in a linear potential, with the spatial period of the oscillations which decreases as n_0 increases owing to the increase of the local slope of the centrifugal potential. An inspection of Eq. (21) clearly shows that for normal beam incidence ($\theta_0=0$), one has $E\geq E_c$ and therefore one always observes Bloch-like oscillations at any beam spatial displacement n_0, whereas for $\theta_0\sim\theta_B$ and n_0 small enough, one observes harmonic oscillations. This behavior can be physically understood by observing that, as it is well known, the sign of discrete diffraction for a broad light beam propagating along a waveguide array strongly depends on the beam incidence angle (see Refs. 20 and 51). For normal beam incidence, the sign of discrete diffraction is the same as in a homogeneous dielectric medium, and therefore the inverted (antiguiding) parabolic potential due to the centrifugal force cannot confine light around the central waveguide: light confinement at the sides of the central waveguide is provided in this case by Bragg reflection. Conversely, for a beam incidence angle close to the Bragg angle, the sign of discrete diffraction is reversed and the waveguide system, near to the central waveguide, behaves like a (confining) parabolic graded-index lens.

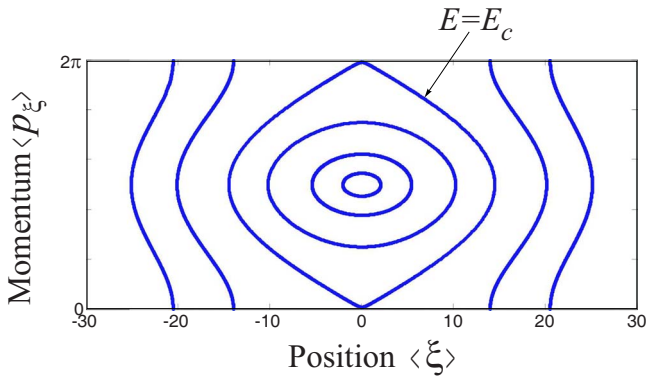

FIG. 2. (Color online) Phase space trajectories of the Hamiltonian system [Eqs. (17) and (18)] (classical pendulum) for $\gamma/\Delta=0.0191$ and for increasing values of energy ($E/E_c=-0.96$, -0.72, 0.42, 1, 2.86, and 5 from the inner to the outer orbits). The separatrix between closed ($E<E_c$) and open ($E>E_c$) orbits corresponds to $E=E_c$.

We checked the above dynamical scenario of discrete diffraction in a helical one-dimensional waveguide array by direct numerical simulations of the paraxial wave equation [Eq. (3)] in the rotating reference frame (x,y,z) using a standard pseudospectral beam propagation technique. In the numerical simulations, we assumed for the refractive index of the single waveguide a circular Gaussian profile of radius r_0 and peak index change Δn, i.e., $n_g(x,y)=n_s+\Delta n\exp[-(x^2+y^2)/r_0^2]$. The waveguide array is excited at the input plane by an elliptical Gaussian beam, broaden in the x direction to excite a few waveguides (typically three to five) of the array.

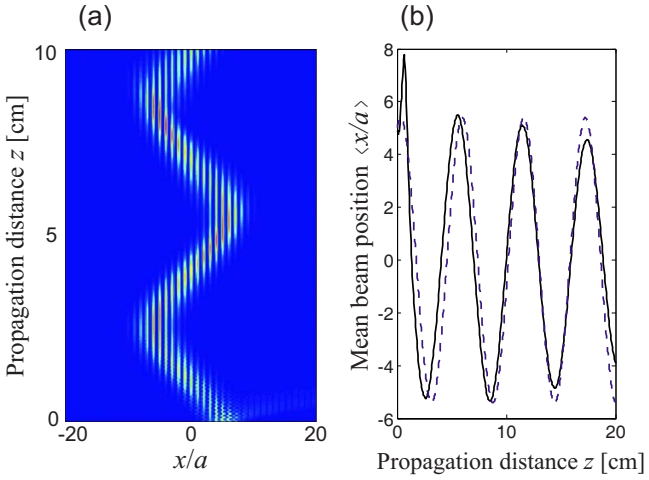

FIG. 3. (Color online) (a) Numerically computed beam propagation in a helical one-dimensional waveguide array corresponding to quasiharmonic oscillations around the central waveguide $n=0$. The figure shows in a colored scale the evolution along the propagation distance z of the integrated beam intensity distribution $\int dy|\psi(x,y,z)|^2$. An elliptic Gaussian beam, broaden in the transverse x direction, centered at the waveguide $n_0=5$ of the array and tilted by an angle $\theta_0=\theta_B/1.1$, has been assumed at the input plane. The values of other parameters are given in the text. (b) Evolution of beam center of mass $\langle\xi\rangle=\langle x/a\rangle$ versus propagation distance as predicted by the full numerical analysis (solid curve) and by the semiclassical analysis (dashed curve) for $\Delta=0.419$ mm^{-1} and $\gamma=0.008$ mm^{-1}.

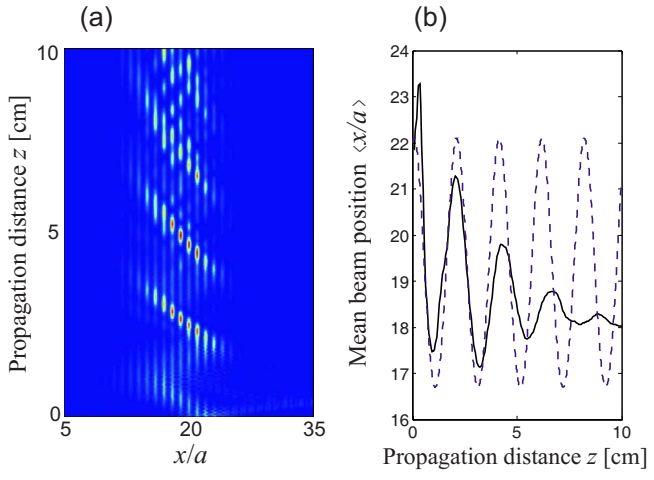

FIG. 4. (Color online) Same as Fig. 3, but for an exciting Gaussian beam centered at the $n_0=22$ waveguide of the array. In this case, $E>E_c$ and the beam undergoes Bloch oscillations.

The different regimes of beam propagation, corresponding to either harmonic or Bloch oscillations, have been investigated by scanning the exciting beam in the transverse x direction (to excite a group of waveguides at around the central waveguide n_0) at a fixed tilting angle θ_0. In order to mainly excite the first band of the array, the tilting angle has been chosen below the Bragg angle θ_B (see, for instance, Refs. 18, 52, and 53). As an example, Figs. 3 and 4 show the numerically computed beam propagation along a $L=10$-cm-long array in the regimes of harmonic oscillations (Fig. 3, corresponding to $n_0=5$) and of Bloch oscillations (Fig. 4, corresponding to $n_0=22$). The parameter values used in the simulations are $\lambda=0.98$ μm, $n_s=1.522$, $a=8.6$ μm, $\Delta n=0.01$, $r_0=3$ μm, $\theta_B/\theta_0=1.1$, and $\Lambda=4$ cm. Note that, contrary to the predictions of the semiclassical analysis, the beam oscillations are in both cases smeared out [see Figs. 3(b) and 4(b)]. This is due to quantum dephasing,[54] i.e., to the nonequidistant spectrum of the quantum pendulum (see, for instance, Ref. 44), which produces beam shape distortion and decay of the oscillations.

IV. LIGHT PROPAGATION IN A TWO-DIMENSIONAL HELICAL ARRAY: THE CLASSICAL ANALOG OF BLOCH MOTION IN A MAGNETIC FIELD

As a second example of quantum-optical correspondence, let us consider light propagation in a periodic two-dimensional helical waveguide array [see Fig. 1(b)]. Owing to Eq. (5), the beam propagation problem in the twisted reference frame (x,y,z) is formally analogous to the quantum mechanical motion of an electron in a two-dimensional crystalline potential under the action of an electromagnetic field. This problem is well known in the solid state physics context (see, for instance, Ref. 28 and 29). Assuming that the electromagnetic potentials vary slowly in space over one lattice constant and are not too strong such that to neglect interband transitions, the motion of a Bloch particle in an electromagnetic field was solved in a rather general and rigorous manner by Luttinger.[34] The approach and results of Luttinger's theory can be briefly reviewed and translated into the optical language as follows. Let us assume that the launching beam at the input plane $z=0$ excites mainly one band of the array, and that interband transitions are negligible.[55] We can then expand the field envelope $\psi(\mathbf{r},z)$ in series of the Wannier functions $W(\mathbf{r}-\mathbf{R}_\rho)$ of the band, displaced at the various lattice sites $\mathbf{R}_\rho$, according to

$$\psi(\mathbf{r},z)=\sum_{\mathbf{R}_\rho} f(\mathbf{R}_\rho,z)W(\mathbf{r}-\mathbf{R}_\rho)\exp\left[i\frac{q}{\chi}\int_{\mathbf{R}_\rho}^{\mathbf{r}}\mathbf{A}(\mathbf{r}')\cdot d\mathbf{r}'\right], \tag{22}$$

where the integral of the vector potential in the exponent on the right hand side of Eq. (22) has to be taken along the straight line correcting the points $\mathbf{R}_\rho$ and $\mathbf{r}$ in the (x,y) plane. The evolution equations for the expansion coefficients $f(\mathbf{R}_\rho,z)$, as obtained by substitution of ansatz (22) into Eq. (5), read explicitly[34]

$$i\chi\frac{\partial f(\mathbf{R}_{\rho'},z)}{\partial z}=\sum_{\mathbf{R}_\rho} E(\mathbf{R}_\rho-\mathbf{R}_{\rho'})f(\mathbf{R}_\rho,z)\exp(i\phi_{\rho'\rho}) + q\varphi(\mathbf{R}_{\rho'})f(\mathbf{R}_{\rho'},z), \tag{23}$$

where

$$\phi_{\rho\rho'} = \frac{q}{\hbar}\int_{\mathbf{R}_\rho}^{\mathbf{R}_{\rho'}} \mathbf{A}(\mathbf{r}')\cdot d\mathbf{r}' \tag{24}$$

are Peierls' phases and $E(\mathbf{R}_\rho)$ the Fourier coefficients of the energy band dispersion curve $E(\mathbf{k})$,

$$E(\mathbf{k}) = \sum_{\mathbf{R}_\rho} E(\mathbf{R}_\rho)\exp(-i\mathbf{k}\cdot\mathbf{R}_\rho). \tag{25}$$

Note that Eq. (23) represents a generalization of the coupled-mode equations [Eq. (9)] derived in Sec. II B. The solution to Eq. (23) is given by $f(\mathbf{R}_{\rho'},z)=f(\mathbf{r}=\mathbf{R}_{\rho'},z)$, where the continuous envelope $f(\mathbf{r},z)$ satisfies the effective Schrödinger equation,

$$i\hbar\frac{\partial f}{\partial z} = E\left(-i\nabla_{\mathbf{r}} - \frac{q\mathbf{A}(\mathbf{r})}{\hbar}\right)f + q\varphi(\mathbf{r})f, \tag{26}$$

with the effective two-dimensional Hamiltonian,[34]

$$\mathcal{H}_{eff}(\mathbf{K},\mathbf{r}) = E(\mathbf{K}) + q\varphi(\mathbf{r}), \tag{27}$$

where $\mathbf{K}=\mathbf{p}/\hbar-q\mathbf{A}(\mathbf{r})/\hbar$ and $\mathbf{p}\equiv-i\hbar\nabla_{\mathbf{r}}$ is the momentum operator. The semiclassical equations of motion for the mean values of beam position $\langle\mathbf{r}\rangle$ and beam momentum $\langle\mathbf{p}\rangle/\hbar$ are given by the Ehrenfest theorem and can be cast in the form[34,56]

$$\hbar\frac{d\langle\mathbf{r}\rangle}{dz} = \nabla_{\mathbf{K}}E(\langle\mathbf{K}\rangle), \tag{28}$$

$$\hbar\frac{d\langle\mathbf{K}\rangle}{dz} = q\mathbf{E}(\langle\mathbf{r}\rangle) + q\frac{d\langle\mathbf{r}\rangle}{dz}\times\mathbf{B}(\langle\mathbf{r}\rangle), \tag{29}$$

where $\mathbf{E}=-\nabla_{\mathbf{r}}\varphi$ and $\mathbf{B}=\nabla_{\mathbf{r}}\times\mathbf{A}$ are the electric and magnetic fields.

As an example, consider a square lattice of optical waveguides, as shown in Fig. 1(b), with lattice size a. The lattice sites are $\mathbf{R}_\rho=na\mathbf{u}_x+ma\mathbf{u}_y$, where $\rho=(n,m)$ and n,m are arbitrary integers. Considering the lowest band of the lattice, in the tight-binding approximation the energy dispersion curve of the band is given by

$$E(\mathbf{k}) = -2\hbar\Delta[\cos(k_x a)+\cos(k_y a)], \tag{30}$$

where $\Delta>0$ determines the bandwidth. Taking into account the expression of the scalar and vector potentials given by Eq. (6), the coupled-mode equations [Eq. (23)] then take the explicit form

$$\begin{aligned} i\frac{\partial f_{n,m}}{\partial z} = &-\Delta[f_{n,m+1}\exp(-i\sigma n) + f_{n,m-1}\exp(i\sigma n) \\ &+ f_{n+1,m}\exp(i\sigma m) + f_{n-1,m}\exp(-i\sigma m)] \\ &- \gamma(n^2+m^2)f_{n,m}, \end{aligned} \tag{31}$$

where γ is given by Eq. (14) and where we have set

$$\sigma = \frac{n_s\epsilon a^2}{\hbar}, \tag{32}$$

and $f_{n,m}(z)=f(\mathbf{R}_{(n,m)},z)$. Note that, in absence of Peierls' phase factors $\exp(\pm i\sigma m)$ and $\exp(\pm i\sigma n)$ that account for the presence of the magnetic field $\mathbf{B}$, the solution to Eq. (31) would be separable $f_{n,m}=c_n g_m$, where c_n and g_m satisfy the one-dimensional quantum harmonic oscillator equation on a lattice [Eq. (12)] considered in the previous section. In the two-dimensional array, however, the magnetic field accounted for by Peierls' phase factors cannot be neglected, and correspondingly, the propagation of a light beam is more involved as compared to the one-dimensional case since, in addition to the electric (centrifugal) force, one has to account for the magnetic (Coriolis) force. At first approximation, the propagation of the center of mass of a broad light beam as a result of the interplay between the electric and magnetic forces can be captured by a semiclassical analysis. From Eqs. (28)–(30), one readily obtains

$$\frac{d\langle n\rangle}{dz} = 2\Delta\sin(\langle P_n\rangle), \tag{33}$$

$$\frac{d\langle m\rangle}{dz} = 2\Delta\sin(\langle P_m\rangle), \tag{34}$$

$$\frac{d\langle P_n\rangle}{dz} = 2\gamma\langle n\rangle + 4\sigma\Delta\sin(\langle P_m\rangle), \tag{35}$$

$$\frac{d\langle P_m\rangle}{dz} = 2\gamma\langle m\rangle - 4\sigma\Delta\sin(\langle P_n\rangle), \tag{36}$$

where we have set $\langle n\rangle=\langle x/a\rangle$, $\langle m\rangle=\langle y/a\rangle$, $\langle P_n\rangle=\langle aK_x\rangle$, and $\langle P_m\rangle=\langle aK_y\rangle$. Note that if the magnetic force were neglected, i.e., if we set $\sigma=0$ in Eqs. (33)–(36), the motion of the beam center of mass in the x and y directions is separable and follows, in each of the two directions, the dynamical behavior of the classic pendulum described in the previous section. In particular, for initial conditions corresponding to beam incidence near the Bragg angle ($\langle P_n\rangle\sim\pi$, $\langle P_m\rangle\sim\pi$) and for an initial beam spatial displacement not too far from the central waveguide $n=m=0$ of the lattice, one would observe two-dimensional quasiharmonic oscillations corresponding to elliptical trajectories of the beam center of mass in the transverse plane. In presence of a non-negligible magnetic force, the trajectories deviate from simple elliptical shape and are more involved [see, for instance, the trajectory shown in Fig. 6(a), to be commented below].

In order to highlight the role played by the magnetic force in the beam propagation dynamics, we numerically integrated the paraxial wave equation [Eq. (3)] in the rotating reference frame (x,y,z), assuming the square lattice waveguide structure of Fig. 1(b). Each waveguide in the lattice has the same Gaussian refractive index profile as in the one-dimensional array considered in Sec. III. The values of parameters for the array, such as lattice constant a, array length L, light wavelength λ, etc., are the same as in Sec. III. The waveguide array is excited at the input plane by a broad circular Gaussian beam, centered at the waveguide (n_0,m_0) of the lattice and with a plane wave front tilted with respect to the (x,y) plane according to the relation

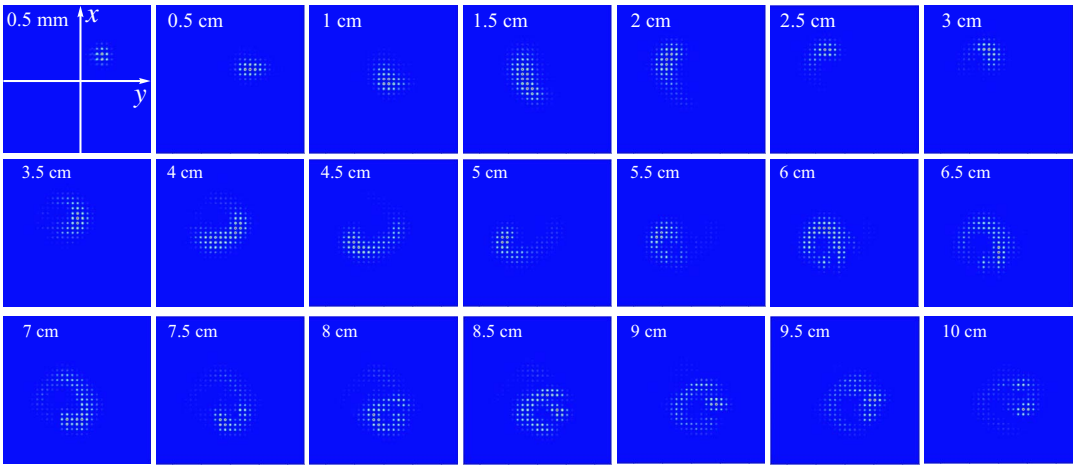

FIG. 5. (Color online) Beam propagation in a helical square lattice waveguide array. The 21 frames show the transverse intensity beam distributions, in the (x,y) plane, at successive propagation distances z indicated in the label of each picture. The size of the square transverse domain in each plot is 130×130 μm^2; the waveguide $n=m=0$, around which the array is twisted, is placed at the center of the square domains. Parameter values are given in the text.

$$\psi(x,y,0) = \exp\left[-\frac{(x-n_0a)^2+(y-m_0a)^2}{w_0^2}\right] \times \exp(-i\theta_{0x}x/\chi - i\theta_{0y}y/\chi), \tag{37}$$

where w_0 is the beam spot size and θ_{0x} and θ_{0y} are the tilting angles. To mainly excite the lowest-order band of the square lattice, the titling angles θ_{0x} and θ_{0y} are assumed smaller than the Bragg angle θ_B. As an example, Fig. 5 shows the detailed evolution of transverse beam intensity distribution, at successive propagation distances, as obtained by numerical simulations of Eq. (3) for parameter values $w_0=2a=17.2$ μm, $n_0=m_0=5$, and $\theta_{0x}/\theta_B=\theta_{0y}/\theta_B=1/1.1$. In the absence of the magnetic field, for these values of parameters, one would observe two-dimensional harmonic oscillations of the beam as in Fig. 3. The results of beam propagation as obtained by a numerical analysis of the coupled-mode equations [Eq. (31)] in the single-band and tight-binding approximations turn out to reproduce very well the complex dynamical evolution shown in Fig. 5. The numerically computed trajectory of the beam center of mass is shown in Fig. 6 (solid lines) and compared with the one predicted by the semiclassical equations [Eqs. (33)–(36)] (dashed lines in the figure). Note that at short propagation distances, the numerically computed beam trajectory follows rather well the complex flowerlike path predicted by the semiclassical analysis; however, a damping of the oscillations is clearly visible at longer propagation distances [see Figs. 6(b) and 6(c)] which is not captured by the semiclassical analysis. As discussed in Sec. III for the quantum harmonic oscillator on a lattice, the damping may be ascribed to quantum dephasing. Note also that quantum dephasing leads to a strong deformation of the beam envelope from Gaussian, with a tendency of spiraling. In any case, the clear flowerlike trajectory followed by the beam center of mass, shown in Fig. 6(a), is a clear signature of the action of the magnetic (Coriolis) force in addition to the electric (centrifugal) force and resembles the cyclotronic motion of a classical particle in a uniform magnetic field. In fact, in the absence of the magnetic field, the path predicted by the semiclassical analysis would be a segment on the bisectrix of the (x,y) plane, represented by the dotted segment in Fig. 6(a), whereas in the absence of the electric field, the beam trajectory would be circular (cyclotronic motion).

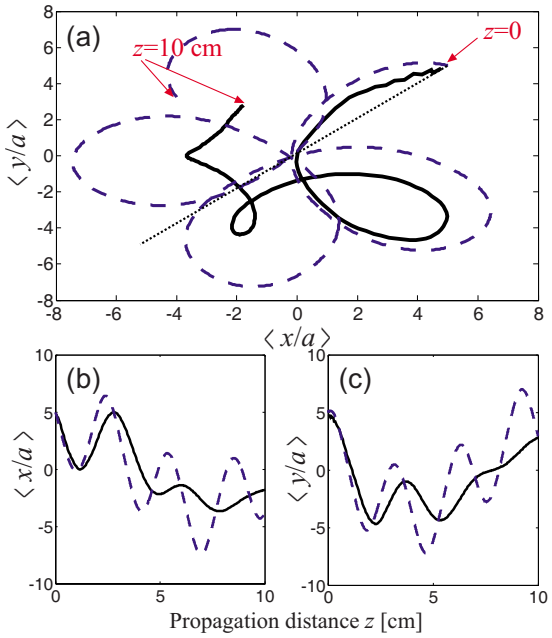

FIG. 6. (Color online) (a) Trajectory of the beam center of mass in the $(\langle x/a\rangle, \langle y/a\rangle)$ plane corresponding to beam propagation in the 10-cm-long helical waveguide array of Fig. 5. The detailed behavior of $\langle x/a\rangle$ and $\langle y/a\rangle$ versus propagation distance z is shown in (b) and (c). Solid lines refer to full numerical simulations of Eq. (3), whereas dashed curves are obtained by solving the semiclassical equations [Eqs. (33)–(36)] with $\Delta=0.419$ mm^{-1}, $\gamma=0.008$ mm^{-1}, and $\sigma=0.1134$. In (a), the dotted segment on the bisectrix is the trajectory of the two-dimensional harmonic oscillations that one would observe in the absence of the magnetic force.

V. CONCLUSIONS

In this work, the classical-quantum analogy between discrete diffraction of light waves in optical waveguide arrays and quantum dynamics of a Bloch electron in an external electric field, investigated in recent theoretical and experimental works,[3,5–12,15–19,22] has been extended to include the effects of a *magnetic* field. In the optical system, the temporal evolution of the electronic wave packet is mimicked by the spatial propagation of the optical beam in the waveguide structure, whereas the effects of electric and magnetic fields are simulated by noninertial forces acting on optical rays of geometric origin. As a geometric bent of the waveguide array along the paraxial propagation direction is capable of simulating the effect of a uniform dc or ac electric field, a possibility theoretically proposed and experimentally demonstrated in recent publications (see, e.g., Refs. 6, 9, 10, 12, 17–19, and 22), in this work it has been shown that a waveguide array with a helical structure can be used to mimic the effect of a uniform magnetic field, superimposed to a (repulsive) harmonic electrostatic force. The magnetic and electric forces are provided by the Coriolis and centrifugal forces experienced by optical rays in the noninertial reference frame rotating with the twisted array (see Sec. II). In case of a one-dimensional helical waveguide array, the magnetic force does not play any role, and discrete diffraction in the array exactly mimics the dynamics of a quantum harmonic oscillator on a lattice (see Sec. III). In two-dimensional helical arrays, light beam propagation is strongly influenced by the additional magnetic force, the effect of which is clearly visible by the appearance of a flowerlike trajectory of the optical beam in the transverse plane according to the semiclassical motion of a Bloch electron in the combined electric and magnetic fields (see Sec. IV). For an experimental observation of such effects, one needs to manufacture high-quality arrays of waveguides or fibers with an helical axis. High-quality two-dimensional arrays of waveguides or fibers with a straight axis have been already demonstrated in recent experiments.[24–27] The helical structure might be obtained by twisting a two-dimensional fiber array[24] or by directly realizing on a glass substrate three-dimensional helically shaped waveguides using the recently developed femtosecond laser writing technique, which enables to manufacture periodic structures of arbitrary two-dimensional geometry.[25–27]

[1] S. Somekh, E. Garmire, A. Yariv, H. L. Garvin, and R. G. Hunsperger, Appl. Phys. Lett. **22**, 46 (1973).

[2] A. Yariv, *Optical Electronics*, 4th ed. (Saunders College, New York, 1991), pp. 519–529.

[3] D. N. Christodoulides, F. Lederer, and Y. Silberberg, Nature (London) **424**, 817 (2003).

[4] T. Schwartz, G. Bartal, S. Fishman, and M. Segev, Nature (London) **446**, 52 (2007).

[5] U. Peschel, T. Pertsch, and F. Lederer, Opt. Lett. **23**, 1701 (1998).

[6] G. Lenz, I. Talanina, and C. M. de Sterke, Phys. Rev. Lett. **83**, 963 (1999).

[7] R. Morandotti, U. Peschel, J. S. Aitchison, H. S. Eisenberg, and Y. Silberberg, Phys. Rev. Lett. **83**, 4756 (1999).

[8] T. Pertsch, P. Dannberg, W. Elflein, A. Bräuer, and F. Lederer, Phys. Rev. Lett. **83**, 4752 (1999).

[9] G. Lenz, R. Parker, M. C. Wanke, and C. M. de Sterke, Opt. Commun. **218**, 87 (2003).

[10] S. Longhi, Opt. Lett. **30**, 2137 (2005).

[11] H. Trompeter, T. Pertsch, F. Lederer, D. Michaelis, U. Streppel, A. Brauer, and U. Peschel, Phys. Rev. Lett. **96**, 023901 (2006).

[12] N. Chiodo, G. Della Valle, R. Osellame, S. Longhi, G. Cerullo, R. Ramponi, P. Laporta, and U. Morgner, Opt. Lett. **31**, 1651 (2006).

[13] G. Della Valle, S. Longhi, P. Laporta, P. Biagioni, L. Duó, and M. Finazzi, Appl. Phys. Lett. **90**, 261118 (2007).

[14] One should mention that the optical analogs of Bloch oscillations and Zener tunneling have been also predicted and experimentally observed in optical superlattices [see, for instance, R. Sapienza, P. Costantino, D. Wiersma, M. Ghulinyan, C. J. Oton, and L. Pavesi, Phys. Rev. Lett. **91**, 263902 (2003); V. Agarwal, J. A. del Rio, G. Malpuech, M. Zamfirescu, A. Kavokin, D. Coquillat, D. Scalbert, M. Vladimirova, and B. Gil, *ibid.* **92**, 097401 (2004); M. Ghulinyan, C. J. Oton, Z. Gaburro, L. Pavesi, C. Toninelli, and D. S. Wiersma, *ibid.* **94**, 127401 (2005)]. The use of coupled-optical waveguides, however, offers the rather unique advantage of permitting a visualization in real space of the dynamical evolution of light waves (see Refs. 11 and 13).

[15] H. Trompeter, W. Krolikowski, D. N. Neshev, A. S. Desyatnikov, A. A. Sukhorukov, Yu. S. Kivshar, T. Pertsch, U. Peschel, and F. Lederer, Phys. Rev. Lett. **96**, 053903 (2006).

[16] A. Fratalocchi, G. Assanto, K. A. Brzdakiewicz, and M. A. Karpierz, Opt. Lett. **31**, 790 (2006).

[17] S. Longhi, M. Marangoni, M. Lobino, R. Ramponi, P. Laporta, E. Cianci, and V. Foglietti, Phys. Rev. Lett. **96**, 243901 (2006).

[18] S. Longhi, M. Lobino, M. Marangoni, R. Ramponi, P. Laporta, E. Cianci, and V. Foglietti, Phys. Rev. B **74**, 155116 (2006).

[19] R. Iyer, J. S. Aitchison, J. Wan, M. M. Dignam, and C. M. de Sterke, Opt. Express **15**, 3212 (2007).

[20] H. S. Eisenberg, Y. Silberberg, R. Morandotti, and J. S. Aitchison, Phys. Rev. Lett. **85**, 1863 (2000).

[21] I. L. Garanovich, A. A. Sukhorukov, and Yu. S. Kivshar, Phys. Rev. E **74**, 066609 (2006).

[22] I. L. Garanovich, A. Szameit, A. A. Sukhorukov, T. Pertsch, W. Krolikowski, S. Nolte, D. Neshev, A. Tuennermann, and Y. S. Kivshar, Opt. Express **15**, 9737 (2007).

[23] S. Longhi, D. Janner, M. Marano, and P. Laporta, Phys. Rev. E **67**, 036601 (2003).

[24] U. Ropke, H. Bartelt, S. Unger, K. Schuster, and J. Kobelke, Opt. Express **15**, 6894 (2007).

[25] S. Nolte, M. Will, J. Burghoff, and A. Tuennermann, Appl. Phys. A: Mater. Sci. Process. **77**, 109 (2003).

[26] T. Pertsch, U. Peschel, F. Lederer, J. Burghoff, M. Will, S. Nolte, and A. Tunnermann, Opt. Lett. **29**, 468 (2004).

[27] A. Szameit, D. Blomer, J. Burghoff, T. Pertsch, S. Nolte, and A. Tunnermann, Appl. Phys. B: Lasers Opt. **82**, 507 (2006).

[28] N. W. Ashcroft and N. D. Mermin, *Solid State Physics* (Saunders, Philadelphia, 1976), Chap. 12.
[29] J. Callaway, *Quantum Theory of the Solid State* (Academic, New York, 1974), Pt. B, Chap. 6.
[30] F. Bloch, Z. Phys. **52**, 555 (1928).
[31] H. Jones and C. Zener, Proc. R. Soc. London, Ser. A **144**, 101 (1934).
[32] R. Peierls, Z. Phys. **80**, 763 (1933).
[33] J. C. Slater, Phys. Rev. **76**, 1592 (1949).
[34] J. M. Luttinger, Phys. Rev. **84**, 814 (1951).
[35] G. Nenciu, Rev. Mod. Phys. **63**, 91 (1991).
[36] S. Longhi, G. Della Valle, and D. Janner, Phys. Rev. E **69**, 056608 (2004).
[37] M. Ornigotti, G. D. Valle, D. Gatti, and S. Longhi, Phys. Rev. A **76**, 023833 (2007).
[38] E. Chalbaud, J.-P. Gallinar, and G. Mata, J. Phys. A **19**, L385 (1986).
[39] J.-P. Gallinar and E. Chalbaud, Phys. Rev. B **43**, 2322 (1991).
[40] C. H. Hooley and J. Quintanilla, Phys. Rev. Lett. **93**, 080404 (2004).
[41] L. Pezzé, L. Pitaevskii, A. Smerzi, S. Stringari, G. Modugno, E. De Mirandes, F. Ferlaino, H. Ott, G. Roati, and M. Inguscio, Phys. Rev. Lett. **93**, 120401 (2004).
[42] H. Ott, E. de Mirandes, F. Ferlaino, G. Roati, V. Türck, G. Modugno, and M. Inguscio, Phys. Rev. Lett. **93**, 120407 (2004).
[43] A. M. Rey, G. Pupillo, C. W. Clark, and C. J. Williams, Phys. Rev. A **72**, 033616 (2005).
[44] J. Brand and A. R. Kolovsky, Eur. Phys. J. D **41**, 331 (2007).
[45] P. B. Blakie, A. Bezett, and P. Buonsante, Phys. Rev. A **75**, 063609 (2007).
[46] Such a situation occurs, for instance, for laser-written waveguiding structures in glass (see, for instance, Refs. 12, 26, and 27).
[47] S. Longhi, Phys. Rev. A **71**, 055402 (2005).
[48] Y. V. Kartashov, B. A. Malomed, and L. Torner, Phys. Rev. A **75**, 061602(R) (2007).
[49] P. Wilkinson and M. Fromhold, Opt. Lett. **28**, 1034 (2003).
[50] In Bose-Einstein condensates, the existence of closed and open orbits corresponds to a crossover from a conduction to an insulating behavior of the condensate. The closed orbits correspond to standard dipolar oscillations of the condensate in an harmonic trap, whereas open orbits correspond to Bloch oscillations of the condensate (see Ref. 41).
[51] T. Pertsch, T. Zentgraf, U. Peschel, A. Bräuer, and F. Lederer, Phys. Rev. Lett. **88**, 093901 (2002).
[52] A. A. Sukhorukov, D. Neshev, W. Krolikowski, and Y. S. Kivshar, Phys. Rev. Lett. **92**, 093901 (2004).
[53] R. Morandotti, D. Mandelik, Y. Silberberg, J. S. Aitchison, M. S. Demetrios, N. Christodoulides, A. A. Sukhorukov, and Y. S. Kivshar, Opt. Lett. **29**, 2890 (2004).
[54] Quantum dephasing, leading to damping of oscillations, can be accounted for in the semiclassical analysis by averaging over an ensemble of trajectories with initial conditions scattered over a suitable volume in the phase space (see Refs. 41 and 44).
[55] If the beam excites more than one band of the waveguide array, the initial beam splits into several wave packets, belonging to the different bands of the array. Neglecting interband transitions, these wave packets propagate indepenedently along the array and at any propagation plane z the overall field distribution is given by the superposition (interference) of the various wave packets (see, for instance, Ref. 18).
[56] In writing the semiclassical equations, we follow Luttinger's theory (Ref. 34) and neglect higher-order correction terms, such as the magnetic moment correction to the energy and the Hall velocity term [see, for instance, G. Sundaram and Q. Niu, Phys. Rev. B **59**, 14915 (1999)].